# Structure and Optical Properties of $K_{0.67}Rb_{1.33}Al_2B_2O_7$ Crystal

**Qian Huang [1,2], Lijuan Liu [1,\*], Mingjun Xia [1], Yi Yang [1,2], Shu Guo [1,2], Xiaoyang Wang [1], Zheshuai Lin [1] and Chuangtian Chen [1]**

[1] Beijing Center for Crystal Research and Development, Key Laboratory of Functional Crystals and Laser Technology, Technical Institute of Physics and Chemistry, Chinese Academy of Sciences, Beijing 100190, China; huangqian112@mails.ucas.ac.cn (Q.H.); xiamingjun@mail.ipc.ac.cn (M.X.); yangyi114@mails.ucas.ucas.ac.cn (Y.Y.); guoshu@mails.ucas.ac.cn (S.G.); xywang@mail.ipc.ac.cn (X.W.); zslin@mail.ipc.ac.cn (Z.L.); cct@mail.ipc.ac.cn (C.C.)

[2] University of the Chinese Academy of Sciences, Beijing 100049, China

\* Correspondence: llj@mail.ipc.ac.cn; Tel.: +86-10-8254-3710

**Abstract:** A UV nonlinear optical (NLO) crystal $K_{0.67}Rb_{1.33}Al_2B_2O_7$ (KRABO) has been obtained by the top-seeded solution growth method for the first time. Its structure is formed of coplanar $[BO_3]^{3-}$ triangle groups and $[Al_2O_7]^{8-}$ groups, which are built from two $[AlO_4]^{5-}$ tetrahedra sharing one vertex. Rb and K atoms have the same coordinates and locate between each layer in a disorderly fashion. The crystal has a larger NLO effect compared with its analog $K_2Al_2B_2O_7$ (KABO), as evidenced by powder second harmonic generation (SHG) test. The shortest SHG phase-matching wavelength is down to 231 nm according to the first-principle calculation, which indicates that KRABO is possible for the fourth harmonic generation of Nd:YAG at 266 nm.

## 1. Introduction

$K_2Al_2B_2O_7$ (KABO) was first reported as a new nonlinear optical crystal by both Hu and Ye in 1998 [1,2]. It crystallizes in the space group of *P*321 with cell parameters a = b = 8.55800(2), c = 8.45576(3) (*z* = 3). It possesses some good nonlinear optical NLO properties, such as a wide transmittance ranging from 180 nm to 3600 nm and a moderate birefringence ($\Delta n = 0.074@1064$ nm) [3–6]. The shortest second harmonic generation (SHG) wavelength is down to 225 nm by type-I phase-matching, so it can be used for the fourth harmonic generation (FOHG) of Nd-based lasers at 266 nm. However, the crystal also has some shortcomings, including extrinsic UV absorption and a small SHG coefficient ($d_{eff} = 0.26$ pm/V). The extrinsic UV absorption of KABO, which is caused by $Fe^{3+}$, can be eliminated by changing the growth atmosphere [7]. The small SHG coefficient is mainly due to the twisting of the $BO_3$ groups between adjacent layers, which partly counteracts the NLO efficiency. This thus pushes researchers to continue modifying the structure to increase the NLO efficiency.

As we know, it is a useful strategy to modify the NLO properties of materials via doping with other ions [8–15]. For example, $BaAlBO_3F_2$ doping with 50% Ga can increase its birefringence, and thus can change the shortest SHG wavelength from 273 nm to 259 nm and be used for the FOHG of Nd-based lasers [16]. Ga-doped KABO as $K_2(Al_{0.71}Ga_{0.29})_2B_2O_7$ (KAGBO) has also been investigated, which shows a slightly smaller SHG coefficient and larger refractive indices [17]. On the contrary, Ga-doped KABO could have absorption in the UV region caused by Ga itself. In this case, KABO doped with ions like Na or Rb without d or f electrons is recommended [18].

Series of Rb-doped $K_{2(1-x)}Rb_{2x}Al_2B_2O_7$ (x = 0.25, 0.5, 0.75) compounds have been studied by Atuchin et al. [19]. The structures have been determined by powders to be in the same space group of *P321* with KABO. With the Rb substitution for K atoms, a noticeable increase of refractive indices was observed [20]. The NLO properties may be improved by Rb ions doping, but no single crystals were obtained yet for optical characterization. It is interesting to grow such crystals for NLO properties evaluation. In this paper, we have successfully grown a single crystal of $K_{0.67}Rb_{1.33}Al_2B_2O_7$ (KRABO). Its crystal growth, structure and optical properties have been evaluated for the first time. Its structure-property relations are also discussed and compared with that of KABO.

## 2. Results and Discussion

### 2.1. Crystal Structure Description

As shown in Figure 1, KRABO crystallizes in the trigonal space group of *P321* with cell parameters of *a* = *b* = 8.6352(12) Å, *c* = 8.6433(17) Å. The parameters of the refinement and atom coordinates of KRABO are shown in Tables S1 and S2, respectively. The structure in the a-b plane is formed by coplanar $[BO_3]^{3-}$ triangle groups and $[Al_2O_7]^{8-}$ groups, which are built from two $[AlO_4]^{5-}$ tetrahedra sharing one vertex. There are three crystallographically independent Al sites forming two different types of distorted $[AlO_4]^{5-}$ groups and one type of apical sharing tetrahedral $[Al_2O_7]^{8-}$ group. It is observed that the two $[AlO_4]^{5-}$ units are almost identical, with the basal Al-O bonds ranging from 1.732 Å to 1.762 Å and the apical Al-O bonds varying from 1.704 Å to 1.736 Å. The bottom surfaces of all of the $[AlO_4]^{5-}$ tetrahedra share corners with three adjacent $BO_3$ triangles to form six-membered rings. These two groups formed a nearly planar $[Al_3B_3O_6]$ framework with all the planes of $BO_3$ groups almost perpendicular to the c axis. K and Rb cations are arranged in the spaces between the layers, which have the same coordinates, and the sum of the partial occupancies is equal to 1. The substitution of Rb atoms with K1 and K2 positions in the KRABO crystal lattice were 0.657/0.343 for Rb1/K1 and 0.612/0.388 for Rb2/K2.
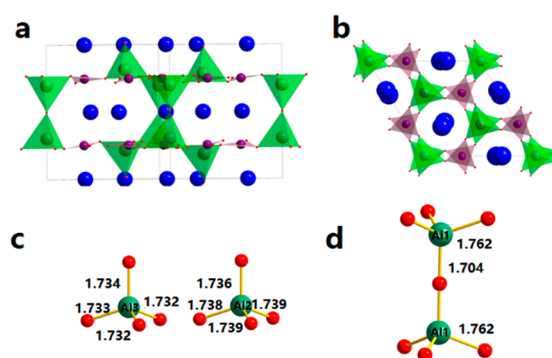


**Figure 1.** (**a**) Crystal structure of KRABO; (**b**) $BO_3$ triangles and $AlO_4$ tetrahedrons in the a-b plane; (**c**) (**d**) the three different types of $AlO_4$ groups.

### 2.2. IR Spectra and Raman Spectra

To investigate the vibration modes of the $BO_3$ and $AlO_4$ groups, both the IR spectrum and Raman spectrum of KRABO were recorded at room temperature and are depicted in Figure 2. The medium strong peaks at about 1050 cm$^{-1}$ in the Raman spectrum and 965 cm$^{-1}$ in the IR spectrum can be ascribed to the symmetric stretching ($\upsilon_1$) of the $BO_3$ group. The weak bands at 1256 cm$^{-1}$ in the Raman spectrum and the middle peaks around 1180–1300 cm$^{-1}$ in the IR spectrum are attributed to the B-O asymmetric stretching ($\upsilon_3$) of the $BO_3$ group. The out-of-plane ($\upsilon_2$) bending and in-plane bending ($\upsilon_4$) of the $BO_3$ group correspond to the 620 cm$^{-1}$ peak in the Raman spectrum. The remaining peaks located at about 118 cm$^{-1}$, 324 cm$^{-1}$, 497 cm$^{-1}$ in the Raman spectrum and 417 cm$^{-1}$, 501 cm$^{-1}$, and around 718–756 cm$^{-1}$ in the IR spectrum can be assigned to the different types of Al-O vibration

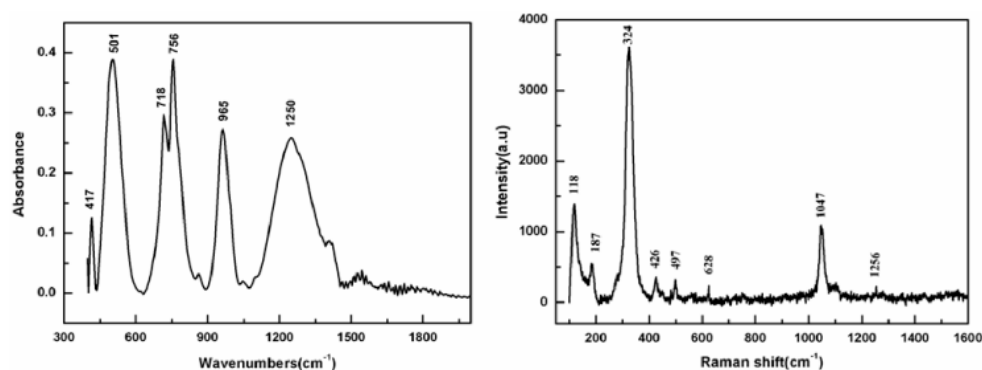modes in KRABO. There are some smaller peaks, which may be due to multi-phonon process of Al-O and B-O groups.



**Figure 2.** IR spectra and Raman spectra of KRABO.

*2.3. Thermal Analysis*

The DSC (Differential Scanning Calorimetry) curve exhibits one endothermic peak on the heating curve at 1130 °C, accompanied by an obvious weight loss observed on the TG (Thermogravimetric Analysis) curve (Figure 3). The XRD pattern indicates that the molten residues were mainly raw materials instead of the original compound, which clearly demonstrates that 1130 °C is the decomposition temperature. Hence, KRABO melts incongruently and must be grown with flux below the decomposition temperature.
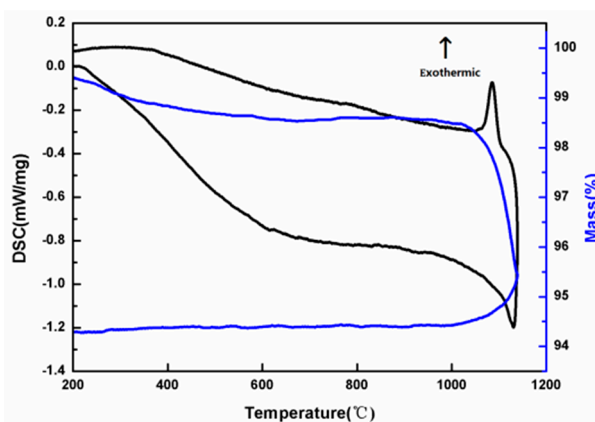


**Figure 3.** DSC and TG curves of KRABO.

*2.4. Transmittance Spectrum*

The transmittance spectrum of KRABO is shown in Figure 4. It is clear that there is no absorption from 400 to 800 nm and the cutoff edge is about 188 nm, which is slightly red-shift compared to that of KABO. The transmittance is about 60% in the visible region, which is due to the inclusions and scattering centers in the grown crystals that seriously reduce the transmittance.
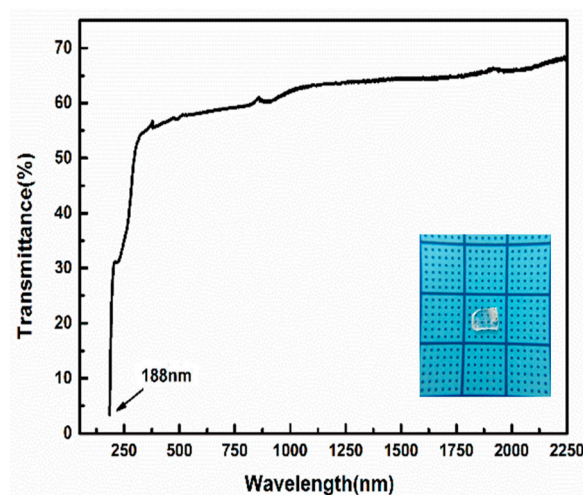
**Figure 4.** The transmittance spectrum of KRABO.

*2.5. NLO Properties*

The plots of the second harmonic intensity versus different particle sizes from the measurements made on ground crystal powders are shown in Figure 5. Based on the Kurtz and Perry rule, we can clearly see that the titled compound is phase-matchable and the SHG intensity is larger than that of KABO. The powder SHG value is about $0.9 \times$ KDP ($KH_2PO_4$) for KRABO and $0.75 \times$ KDP for KABO.
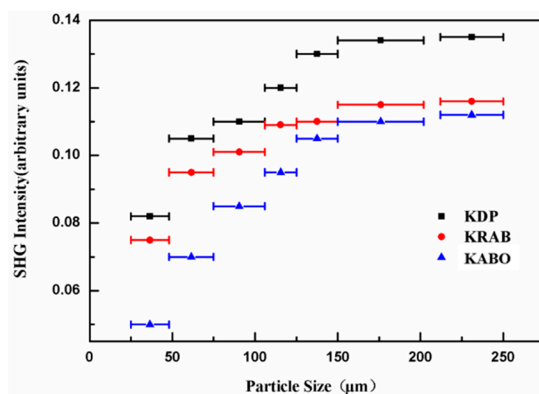


**Figure 5.** SHG intensity vs particle size curves at 1064 nm.

It is meaningful to mention that the SHG effect of KRABO is larger than that of KABO. The reason can be explained from the structure-property relationship. The structure of KRABO is almost the same as KABO, which contains $BO_3$ and $AlO_4$ as basic anionic groups. According to the anionic group theory, which was proposed by Professor Chen in the 1970s [21–23], the overall SHG efficiency is the geometrical superposition of the microscopic second-order susceptibilities of the anionic groups. In KABO, the major contributions to SHG efficiency are from the coplanar $BO_3$ groups and $AlO_4$ groups by first-principles calculations [24]. Since the arrangement of $AlO_4$ groups is almost the same in both KABO and KRABO, we mainly focus on the different arrangement of the $BO_3$ groups in the two structures. The SHG effect is maximized if the $BO_3$ groups are arranged in the same order with a tilt angle of $0°$, and it is minimized if the $BO_3$ groups are arranged in the opposite order with a tilt angle of $60°$. The arrangements of the $BO_3$ groups in both KRABO and KABO are shown in Figure 6. It is found that the twisting angles of $BO_3$ groups between different a-b planes get smaller in KRABO than that in KABO. In KRABO, the twisting angle of each $BO_3$ group is $35.6°$ for the adjacent layers, whereas it is $40.5°$ in KABO. Evidently, the lesser twisting angle of $BO_3$ groups contributes to a larger

SHG effect, which is proved by the powder SHG efficiency test. The structure variety can be explained by Rb ions-doping. In order to host the bigger Rb cations in a K-O lattice, the Al-O bonds become more elongated, and therefore the $BO_3$ group can be less twisted.
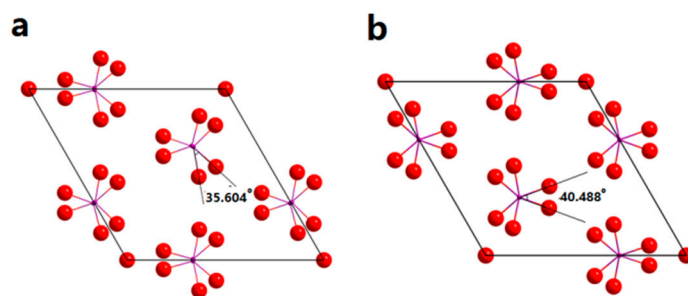


**Figure 6.** Arrangement of $BO_3$ triangles in KRABO (**a**) and KABO (**b**) crystals viewed along the c axis.

### 2.6. Theoretical Calculations

In order to elucidate the mechanism of optical properties, first-principles calculations were performed by the plane-wave pseudopotential method implemented in the CASTEP package. The electronic band structure of the KRABO crystal is shown in Figure 7a, exhibiting the calculated energy band gaps of 3.789 eV. Meanwhile, the density of states (DOS) and the partial density of states (PDOS) projected on the constitutional atoms of the title compounds are shown in Figure 7b, from which the following electronic characteristics are shown: (I) The region lower than $-7$ eV consists of the isolated inner-shell states with Rb 4s4p, K 3p and O 2s orbitals, which have little interactions with neighbor atoms. (II) The upper part of the VB (Valence band) is mainly composed of the p orbitals of O (2p) and B (2p). (III) The bottom part of the CB (Conduction band) is a constituent of the orbitals of all atoms. Since the optical response of a crystal mainly originates from the electronic transitions between the VB and CB states close to the band gap, the B-O group determines the optical properties in the crystal.
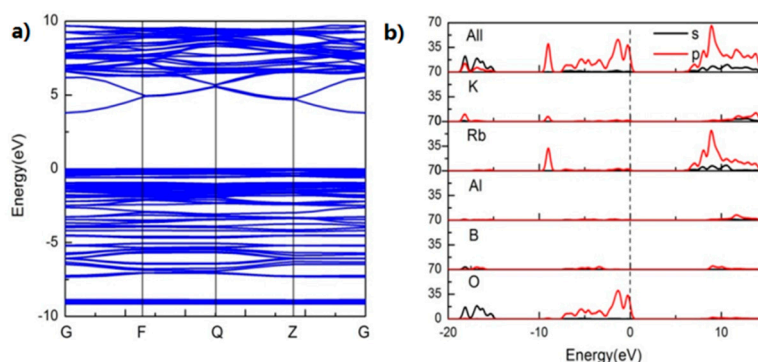


**Figure 7.** (**a**) Electronic band structure; (**b**) DOS and PDOS plots of KRABO.

The first-principles linear and nonlinear optical properties in KRABO are listed in Table S3. Its birefringence index is calculated to be 0.054 at 1064 nm. The shortest SHG phase-matching wavelength is down to 231 nm. By the restriction of Kleinman's symmetry, KRABO has only one nonzero independent SHG coefficient ($d_{11}$) owing to its *P321* space group, which is calculated to be $d_{11} = 0.395$ pm/V ($1.01 \times$ KDP) and is in agreement with the experimental results.

## 3. Materials and Methods

### 3.1. Synthesis and Crystal Growth

Polycrystalline KRABO samples were prepared by solid-state reaction using a mixture of pure $Al_2O_3$ (4N), $H_3BO_3$ (chemically pure grade), $K_2CO_3$ (chemically pure grade), and $Rb_2CO_3$ (chemically pure grade) in stoichiometric ratio as the starting materials. The mixture was ground in an agate mortar and heated at 300 °C initially, then slowly heated to 800 °C and kept for 48 h. The phase purity was confirmed by powder X-ray diffraction (XRD), which matches well with the calculated values (Figure S1). Single crystals were obtained by a high-temperature flux method. Polycrystalline KRABO powders were mixed with $H_3BO_3$ and NaF with a molar ratio of 1:0.5:1.5 in a Pt crucible. The temperature was increased to 800 °C for complete dissolution. The initial crystal was obtained by spontaneous nucleation and then was used as a seed. By a slow cooling rate of 0.5 °C/d, the crystal was grown. After the growth period had finished, the crystal was pulled out from the solution and cooled down to room temperature within three days.

### 3.2. Single-Crystal X-Ray Diffration

Single-crystal X-ray diffraction data was collected using the graphite-monochromatized Mo-K$\alpha$ ($\lambda$ = 0.71073 Å) radiation at 153 K on a Rigaku AFC10 diffractometer (Rigaku Corporation, Tokyo, Japan). The data was integrated using the Crystal Clear program and face-indexed absorption corrections were performed numerically with the program XPPEP. The structure was solved by a direct method using SHELXS-97 (University of Gottingen, Gottingen, Germany) and then refined by a full-matrix least-squares refinement on $F^2$. The structure was verified using the ADDSYM algorithm from the program PLATON.4, and no higher symmetries were found.

### 3.3. Powder X-Ray Diffraction

Powder X-ray diffraction was recorded on a Bruker D8 ADVANCE X-ray diffractometer (Bruker, Berlin, Germany) with Cu K$\alpha$ radiation ($\lambda$ = 1.5418 Å) at room temperature. The scanning range is between 10 and 70° with a scanning width of 0.02 and a rate of $0.1°\ s^{-1}$. The powder XRD pattern for the pure powder sample of KRABO shows good agreement with the XRD pattern calculated from the single-crystal model (see Figure S1).

### 3.4. Thermal Analysis

The thermal property was investigated by differential scanning calorimetric (DSC) analysis and thermogravimetric analysis (TGA) using the NETZSCH STA 449C TG/DSC/DTA thermal analyzer (NETZSCH, Berlin, Germany). A 10 mg powder sample was placed in a Pt crucible and heated from room temperature to 1250 °C at a rate of 10 °C min$^{-1}$ in nitrogen atmosphere.

### 3.5. Transmittance Spectrum

The transmittance spectrum of KRABO crystal with the thickness about 0.15 mm was measured using a Perkin-Elmer Lambda 900 UV-vis-NIR spectrometer (Perkin-Elmer, Woodbridge, ON, Canada) in the range of 185–3000 nm. The interference pattern of KRABO crystal was observed on an Olympus BX51TRF microscope (Olympus, Tyoko, Japan).

### 3.6. Second harmonic Generation

Powder second harmonic generation (SHG) measurements were performed using Kurtz and Perry method [25]. KRABO crystals were ground and sieved into distinct particle size ranges: 25–50, 50–75, 75–100, 100–125, 125–150, 150–200, and 210–250 μm. The sieved KDP powders and KABO powders with the same size were used as references. The samples were irradiated by a Q-switched Nd:YAG laser at 1064 nm (5 ns,1 Hz).

*3.7. Calculation Methods.*

First-principles calculations for KRABO were performed by CASTEP [26], a plane-wave pseudopotential total energy package based on density functional theory (DFT) [27]. This functional theory developed by Perdew-Burke-Emzerhoff (PBE) within the generalized gradient approximation (GGA) [28,29] form was adopted to describe the exchange-correlation energy. The optimized norm-conserving pseudopotentials [30] in the Kleinman-Bylander [31] form for all the elements were used to model the effective interaction between atom cores and valence electrons. Also, K $3s^2 3p^6 4s^1$, Rb $4s^2 4p^6 5s^1$, Al $3s^2 3p^1$, B $2s^2 2p^1$ and O $2s^2 2p^4$ electrons were treated as valence electrons, allowing for the adoption of a relatively small basis set without compromising the computational accuracy. The high kinetic energy cutoff 850 eV and dense $3 \times 3 \times 3$ Monkhorst-Pack [32] *k*-point meshes in the Brillouin zones were chosen for KRABO. Our tests showed that the above computational set ups are sufficiently accurate for the present purposes.

The energy band gaps calculated by standard DFT method are smaller than the measured values, due to the discontinuity of the exchange-correlation energy. The scissor operators were adopted to shift all the conduction bands to match the calculated band gaps with the measured values, where the scissors operator is set as the difference between the experiment and the GGA band gaps. Based on the scissor-corrected electron band structure, the imaginary part of the dielectric function is calculated and the real part of the dielectric function is determined using the Kramers–Kronig transform, from which the refractive indices n (and the birefringence Δn) is obtained. Furthermore, the second order susceptibility $\chi^{(2)}$ and the second harmonic generation (SHG) coefficients $d_{ij}$ are calculated using an expression originally proposed by Rashkeev et al. [33], and developed by Lin et al. [34,35]. The second-order susceptibility $\chi_{ijk}$ is represented as:

$$\chi_{ijk} = \chi_{ijk}(VE) + \chi_{ijk}(VH) + \chi_{ijk}(twobands) \tag{1}$$

where $\chi_{ijk}$ (VE) and $\chi_{ijk}$ (VH) denote the contributions from virtual-electron processes and virtual-hole processes, respectively, and $\chi_{ijk}$ (two bands) gives the contribution from two band processes to $\chi^{(2)}$. The formulas for calculating $\chi_{ijk}$ (VE), $\chi_{ijk}$ (VH) and $\chi_{ijk}$ (two bands) are as follows:

$$\chi_{ijk}(VE) = \frac{e^3}{2\hbar^2 m^3} \sum_{vcc'} \int \frac{d^3k}{4\pi^3} P(ijk) Im\left[p_{vc}^i p_{cc'}^j p_{c'v}^k\right] \left(\frac{1}{\omega_{cv}^3 \omega_{vc'}^2} + \frac{2}{\omega_{vc}^4 \omega_{c'v}}\right), \tag{2}$$

$$\chi_{ijk}(VH) = \frac{e^3}{2\hbar^2 m^3} \sum_{vv'c} \int \frac{d^3k}{4\pi^3} P(ijk) Im\left[p_{vv'}^i p_{v'c}^j p_{cv}^k\right] \left(\frac{1}{\omega_{cv}^3 \omega_{v'c}^2} + \frac{2}{\omega_{vc}^4 \omega_{cv'}}\right), \tag{3}$$

$$\chi_{ijk}(twobands) = \frac{e^3}{\hbar^2 m^3} \sum_{vc} \int \frac{d^3k}{4\pi^3} P(ijk) \frac{Im\left[p_{vc}^i p_{cv}^j (p_{vv}^k - p_{cc}^k)\right]}{\omega_{vc}^5} \tag{4}$$

Here, *i*, *j* and *k* are Cartesian components; *v* and *v′* denote VB, and *c* and *c′* denote CB. *P(ijk)* denotes full permutation. It should be emphasized that the refractive indices and SHG coefficients can be accurately obtained by DFT in principle because these optical properties are determined by the virtual electronic excited processes, which are described by the first and second order perturbations on the ground state wave functions, respectively.

## 4. Conclusions

An NLO crystal, K0.67Rb1.33Al2B2O7 (KRABO), has been grown by high temperature flux method for the first time and its structure and optical properties are discussed. The structure of KRABO is close to that of KABO. With the doping of Rb ions, the twisting angles of BO3 groups between each a-b plane decreases from 40.45° to 35.60°, which is the main contributor to the increase of SHG effects. This provides a new way to improve the SHG effects by ion doping. The title crystal

also possesses a wide transmittance in the range of 188 to 3000 nm and is phase-matchable down to the UV region, which makes it a potential FOHG NLO material.

**Author Contributions:** Qian Huang and Lijuan Liu conceived and designed the experiments; Qian Huang performed the experiments; Yi Yang and Zheshuai Lin contributed to calculation. Mingjun Xia analyzed the crystal data; Shu Guo, Xiaoyang Wang and Chuangtian Chencontributed regent/materials/analysis tools; Qian Huang wrote the paper.

**Conflicts of Interest:** The authors declare no conflict of interest.

## References

1. Hu, Z.G.; Higashiyama, T. A new nonlinear optical borate crystal $K_2Al_2B_2O_7$ (KAB). *J. Appl. Phys.* **1998**, *37*, 1093–1094. [CrossRef]

2. Ye, N.; Zeng, W.R. New nonlinear optical crystal $K_2Al_2B_2O_7$. *J. Opt. Soc. Am. B* **2000**, *17*, 764–768. [CrossRef]

3. Hu, Z.G.; Yoshimura, M.; Mori, Y.; Sasaki, T.; Kato, K. Growth of $K_2Al_2B_2O_7$ crystal for UV light generation. *Opt. Mater.* **2003**, *23*, 353–356. [CrossRef]

4. Zhang, C.; Wang, J.; Cheng, X.; Hu, X.; Jiang, H.; Liu, Y.; Chen, C. Growth and properties of $K_2Al_2B_2O_7$ crystal. *Opt. Mater.* **2003**, *23*, 357–362. [CrossRef]

5. Umemura, N.; Ando, M.; Suzuki, K.; Takaoka, E.; Kato, K.; Hu, Z.-G.; Yoshimura, M.; Mori, Y.; Sasaki, T. 200-mW-average power ultraviolet generation at 0.193 μm in $K_2Al_2B_2O_7$. *Appl. Opt.* **2003**, *42*, 2716–2719. [CrossRef] [PubMed]

6. Kumbhakar, P.; Kobayashi, T. Ultrabroad-band phase matching in two recently grown nonlinear optical crystals for the generation of tunable ultrafast laser radiation by type-I noncollinear optical parametric amplification. *J. Appl. Phys.* **2003**, *94*, 1329–1338. [CrossRef]

7. Liu, C.L.; Liu, L.J. Crystal growth and optical properties of non-UV absorption $K_2Al_2B_2O_7$ crystals. *J. Cryst. Growth* **2011**, *318*, 618–620. [CrossRef]

8. Huang, J.J.; Ji, G.J.; Shen, T.; Andreev, Y.M.; Shaiduko, A.V.; Lanskii, G.V.; Chatterjee, U. Influence of composition ratio variation on optical frequency conversion in mixed crystals. I. Gradual variation of composition ratio. *J. Opt. Soc. Am. B* **2007**, *24*, 2443–2453. [CrossRef]

9. Huang, J.J.; Gao, W.; Shen, T.; Mao, B.L.; Andreev, Y.M.; Shaiduko, A.V.; Lanskii, G.V.; Chatterjee, U.; Atuchin, V.V. Atuchin, Influence of composition ratio variations on optical frequency conversion in mixed crystals. II. Random variation of composition ratio. *J. Opt. Soc. Am. B* **2007**, *24*, 3081–3090. [CrossRef]

10. Wang, Y.; Li, R.K. $K_2Fe_2B_2O_7$: A transparent nonlinear optical crystal with frustrated magnetism. *J. Solid State Chem.* **2010**, *183*, 1221–1225. [CrossRef]

11. Kalabin, I.E.; Shevtsov, D.I.; Azanova, I.S.; Taysin, I.F.; Atuchin, V.V.; Volyntsev, A.B.; Shilov, A.N. Quenching effects on crystallographic and optical properties of H: $LiNbO_3$ layers. *J. Phys. D Appl. Phys.* **2004**, *37*, 1829–1833. [CrossRef]

12. Andreev, Y.M.; Atuchin, V.V.; Lanskii, G.V.; Pervukhina, N.V.; Popov, V.V.; Trocenco, N.C. Linear optical properties of $LiIn(S_{1-x}Se_x)_2$ crystals and tuning of phase matching conditions. *Solid State Sci.* **2005**, *7*, 1188–1193. [CrossRef]

13. He, M.; Kienle, L.; Simon, A.; Chen, X.L.; Duppel, V. Re-examination of the crystal structure of $Na_2Al_2B_2O_7$: Stacking faults and twinning. *J. Solid State Chem.* **2004**, *177*, 3212–3218. [CrossRef]

14. He, M.; Chen, X.; Okudera, H.; Simon, A. $(K_{1-x}Na_x)_2Al_2B_2O_7$ with $0 \leq x < 0.6$: A Promising Nonlinear Optical Crystal. *Chem. Mater.* **2005**, *17*, 2193–2196.

15. Yue, Y.; Wu, Z.; Lin, Z.; Hu, Z. Growth and properties of bulk Na-doped KABO crystals. *Solid State Sci.* **2011**, *13*, 1172–1175. [CrossRef]

16. Yang, L.; Yue, Y. 266 nm ultraviolet light generation in Ga-doped BaAlBO$_3$F$_2$ crystals. *Opt. Lett.* **2016**, *41*, 1598–1600. [CrossRef] [PubMed]

17. Wang, X.; Li, R.K. Growth and optical properties of K$_2$(Al$_{0.71}$Ga$_{0.29}$)$_2$B$_2$O$_7$ crystal. *Opt. Mater.* **2015**, *45*, 197–201. [CrossRef]

18. Wu, Z.; Yue, Y. Growth and optical properties of (K$_{0.62}$Na$_{0.38}$)$_2$Al$_2$B$_2$O$_7$ crystal. *Opt. Mater.* **2012**, *34*, 1575–1578. [CrossRef]

19. Atuchin, V.V.; Bazarov, B.G. Preparation and structural properties of nonlinear optical borates K$_{2(1-x)}$Rb$_{2x}$Al$_2$B$_2$O$_7$, 0 < *x* < 0.75. *J. Alloy. Compd.* **2012**, *515*, 119–122.

20. Atuchin, V.V.; Adichtchev, S.V. Electronic structure and vibrational properties of KRbAl$_2$B$_2$O$_7$. *Mater. Res. Bull.* **2013**, *48*, 929–934. [CrossRef]

21. Chen, C.T. Localized quantal theoretical treatment, based on an anionic coordination polyhedron model, for the EO and SHG effects in crystals of the mixed-oxide types. *Sci. Sin (Engl. Ed.)* **1979**, *22*, 756–776.

22. Chen, C.T.; Liu, G.Z. Recent advances in nonlinear optical and electro-optical materials. *Annu. Rev. Mater. Sci.* **1986**, *16*, 203–243. [CrossRef]

23. Chen, C.T.; Wu, Y.C.; Li, R.K. The anionic group theory of the non-linear optical effect and its applications in the development of new high-quality NLO crystals in the borates series. *Int. Rev. Phys. Chem.* **1989**, *8*, 65–81. [CrossRef]

24. Chen, C.T.; Lin, Z.S.; Wang, Z. The development of new borate-based UV nonlinear crystals. *Appl. Phys. B* **2005**, *80*, 1–25. [CrossRef]

25. Kurtz, S.; Perry, T. A Powder Technique for the Evaluation of Nonlinear Optical Materials. *J. Appl. Phys.* **1968**, *39*, 3798–3813. [CrossRef]

26. Clark, S.J.; Segall, M.D.; Pickard, C.J.; Hasnip, P.J.; Probert, M.J.; Refson, K.; Payne, M.C. First principles methods using CASTEP. *Z. Für Krist.* **2005**, *220*, 567–570. [CrossRef]

27. Payne, M.C.; Teter, M.P.; Allan, D.C.; Arias, T.A.; Joanno-poulos, J.D. Iterative minimization techniques for *ab initio* total-energy calculations: Molecular dynamics and conjugate gradients. *Rev. Mod. Phys.* **1992**, *64*, 1045–1097. [CrossRef]

28. Ceperley, D.M.; Alder, B.J. Ground State of the Electron Gas by a Stochastic Method. *Phys. Rev. Lett.* **1980**, *45*, 566. [CrossRef]

29. Perdew, J.P.; Zunger, A. Self-interaction correction to density-functional approximations for many-electron systems. *Phys. Rev. B* **1981**, *23*, 5048–5079. [CrossRef]

30. Rappe, A.M.; Rabe, K.M.; Kaxiras, E.; Joannopoulos, J.D. Optimized pseudopotentials. *Phys. Rev. B* **1990**, *41*, 1227–1230. [CrossRef]

31. Kleinman, L.; Bylander, D.M. Efficacious Form for Model Pseudopotentials. *Phys. Rev. Lett.* **1982**, *48*, 1425–1428. [CrossRef]

32. Monkhorst, H.J.; Pack, J.D. Special points for Brillouin-zone integrations. *Phys. Rev. B* **1976**, *13*, 5188–5192. [CrossRef]

33. Rashkeev, S.N.; Lambrecht, W.R.L.; Segall, B. Efficient ab initio method for the calculation of frequency-dependent second-order optical response in semiconductors. *Phys. Rev. B* **1998**, *57*, 3905–3919. [CrossRef]

34. Lin, J.; Lee, M.H.; Liu, Z.P.; Chen, C.T.; Pickard, C.J. Mechanism for linear and nonlinear optical effects in beta-BaB$_2$O$_4$ crystals. *Phys. Rev. B* **1999**, *60*, 13380–13389. [CrossRef]

35. Lin, Z.; Jiang, X.; Kang, L.; Gong, P.; Luo, S.; Lee, M.-H. First-principles materials applications and design of nonlinear optical crystals. *J. Phys. D Appl. Phys.* **2014**, *47*, 253001. [CrossRef]